A&A 575, A46 (2015)
DOI: 10.1051/0004-6361/201424758

Astronomy & Astrophysics

Frequencies and mode identifications of the δ Scuti star EE Camelopardalis

M. Breger[1,2], P. Lenz[1,3], A. A. Pamyatnykh[3], V. S. Schmid[1,4], and P. G. Beck[1,4]

[1] Institut für Astrophysik der Universität Wien, Türkenschanzstr. 17, 1180 Wien, Austria
e-mail: michel.breger@univie.ac.at
[2] Department of Astronomy, University of Texas, Austin, TX 78712, USA
[3] N. Copernicus Astronomical Center, Bartycka 18, 00-716 Warsaw, Poland
[4] Instituut voor Sterrenkunde, KU Leuven, Celestijnenlaan 200D, 3001 Leuven, Belgium

Received 5 August 2014 / Accepted 25 November 2014

ABSTRACT

Aims. EE Cam belongs to a group of slightly evolved main-sequence A stars with intermediate rotational velocities. The pulsation frequencies and their mode identification of this star are of interest in order to compare these with those known for the high-amplitude δ Scuti stars (HADS) and the common fast-rotating low-amplitude δ Scuti pulsators.
Methods. The variability of the δ Scuti star EE Cam was observed photometrically for more than 300 nights from 2006 to 2010.
Results. Forty pulsation frequencies are identified, ranging from 3.4 to 13.3 cd^{-1} (40 to 154 μHz). The frequency distribution of the residuals suggests the presence of a large number of additional small-amplitude modes in the same frequency range. We compare the observed phase differences and amplitude ratios with those predicted by pulsation models. The dominant mode at 4.93 cd^{-1} is found to be a radial mode, while the mode at 5.21 cd^{-1} is identified as a nonradial $\ell = 1$ mode. Furthermore, when we compare the frequency range of the detected modes with detailed stellar models of pulsational instability, the radial mode is found to be the fundamental mode.
Conclusions. We have studied and presented the pulsation behavior of EE Cam. It demonstrates that a moderately rotating star can exhibit the behavior of the two groups of δ Scuti stars: the identification of the dominant mode as the radial fundamental is similar to that found in the slowly rotating HADS, and the presence of a very large number of low-amplitude nonradial modes resembles the property of the fast rotating low-amplitude δ Scuti stars.

Key words. stars: variables: δ Scuti – stars: oscillations – techniques: photometric – stars: individual: EE Camelopardalis

1. Introduction

One of the most important physical parameters for determining which pulsation modes are excited in a δ Scuti star is stellar rotation. The majority of δ Scuti stars rotate faster than 50 km s^{-1} and pulsate with low-amplitude nonradial modes. On the other hand, most slowly rotating variables are high-amplitude radial pulsators (the so-called high-amplitude δ Scuti stars, HADS). The division between the HADS and the low-amplitude pulsators is not exact. In fact, the sharp-lined star KIC 9700322, studied with the *Kepler* satellite mission (Koch et al. 2010), has all the properties of a HADS such as slow rotation and dominant radial modes (Breger et al. 2011), but a peak-to-peak amplitude below the 0.3 mag originally defining the HADS group. Nevertheless, statistically speaking, an excellent inverse relationship between the amplitudes of radial and low-degree nonradial pulsation and rotational velocity exists, as demonstrated in Fig. 5 of Breger (2000).

EE Cam belongs to a relatively small group of δ Sct stars with a rotational velocity between the two groups. This intermediate group allows the relationship between pulsational amplitude and rotational velocity to be studied. Koen (2001) reanalyzed the list of pulsators in the HIPPARCOS catalog (Perryman et al. 1997) and suggested two pulsation frequencies for EE Cam. EE Cam was observed photometrically for 304 h in two observing seasons during 2006 and 2007 (Breger et al. 2007, hereafter called Paper I). Fifteen frequencies were derived and the two frequencies found by Koen were confirmed. The rotational velocity was found to be $v \sin i = 40 \pm 3$ km s^{-1}. Detailed line-profile analyses using new high-dispersion spectra (Castanheira et al. 2014) led to the pulsation mode identification of the three photometrically dominant modes as well as a determination of the inclination angle, $i = 34 \pm 4°$. This implies an equatorial rotation velocity of 72 ± 10 km s^{-1} and places EE Cam near the high-rotation limit of the intermediate-rotation group.

2. Photometric observations

From 2006 to 2010, EE Cam was observed photometrically for 300+ nights with the T6 0.75 m Vienna Automatic Photoelectric Telescope (APT), situated at Washington Camp in Arizona (Strassmeier et al. 1997; Breger & Hiesberger 1999). This number includes the 87 nights from 2006 and 2007 analyzed in our previous publication. The telescope has been used before for several other lengthy campaigns of the Delta Scuti Network, which confirmed the long-term stability and millimag precision of the APT photometry. The v and y filters of the Strömgren system were used. For the present analysis, we selected the 275 nights with high-quality data, as judged by the scatter from the comparison stars.

HD 35606 (F8) and HD 37420 (F5) were measured as comparison stars. A third star, HD 32745 (G0), was also observed; since its constancy could not be verified, it was not included in

the final reductions. In the observing sequence of about 9 min, all stars were observed for equal amounts of time. The two comparison stars used agreed with each other to an average of ±3 mmag in both the y and v passbands. Paper I has already presented some sample light curves for the 2006/7 data.

3. Frequency analyses

The pulsation frequency analyses were performed with a package of computer programs with single-frequency and multiple-frequency techniques (PERIOD04, Lenz & Breger 2005). The package utilizes both Fourier and multiple-least-squares algorithms. The latter technique does not rely on sequential prewhitening and fits up to several hundreds of simultaneous sinusoidal variations.

New frequencies of pulsation were searched for by applying Fourier analyses to the data prewhitened by the previously detected frequencies. An illustration with a number of power spectra can be found in Fig. 2 of Paper I. A few frequencies exhibited amplitude variability from year to year. Except for one frequency, no frequency variability was detected. PERIOD04 is able to take care of amplitude and phase variability. During the search for additional frequencies, in order to reduce the number of free parameters, amplitude variability was included only for those modes with clear evidence of such variability (such as f_3). For our search of modes with small amplitudes near 1 mmag, we improved the signal-to-noise ratios by combining the data from the v and y passbands. This was done by scaling the v data by an experimentally determined factor of 0.636 and increasing the statistical weights of the scaled data accordingly. The combining of data taken through two different passbands was used only for the frequency search, but not for the subsequent multifrequency fits. Following Breger et al. (1993), a significance criterion of an amplitude signal-to-noise ratio of 4.0 (which corresponds to a power signal-to-noise ratio ∼12.6) was adopted for all frequencies.

The new observations span a time range of 1495 d. This predicts an excellent frequency resolution near 0.001 d, allowing us to look for close-frequency pairs. This promising situation is compromised somewhat by the presence of annual and daily aliasing, leading to the separations of 0.0027 cd^{-1} and 1 cd^{-1}, respectively.

Forty statistically significant frequencies were detected and are listed in Table 1. The amplitude errors given in the table are the formal errors based on the residuals. Of these 40 frequencies, one pulsation mode caused some problems in our analysis: The 7.91 cd^{-1} peak (f_7) cannot be fit by a single frequency, even with an amplitude change from year to year. The frequency change is so large that it is quite obvious in the Fourier transforms linking the different years. Furthermore, within the 2008/9 observing season, the amplitude increased steadily (see footnote of Table 1). Since close frequencies are common among δ Scuti stars and have been detected in this star, we have attempted to fit two close frequencies to f_7. Our attempts failed. Even a four-frequency model did not provide a satisfactory fit. Consequently, we have assumed a single frequency and determined the best frequency value for each year. These values increase systematically from 7.9051 ± 0.0001 cd^{-1} in the 2006/7 season to 7.9081 ± 0.0001 cd^{-1} in 2009/2010. At this stage we cannot absolutely rule out the presence of multiple modes near that frequency, although we could not isolate them. If f_7 is a single pulsation mode, the relatively large frequency drift would be unusual for a δ Scuti star.

The average residuals of the 40-frequency fit are ±4.0 mmag in the y and ±5.5 mmag in v passbands. These residuals are larger than the ±3 mmag derived from the comparison stars. The reason for this behavior is demonstrated in Fig. 1, which shows the frequency distribution of the residual noise. The noise level of the residuals is highest in the frequency range in which the previously prewhitened pulsation modes are found. The most probable explanation is the combined effects of unrecognized amplitude variability of the known small-amplitude frequencies, f_{13} to f_{40}, as well as the presence of many additional frequencies with amplitudes less than 1.0 mmag.

For the results presented in Table 1, the nine nights from the 2005/6 observing season were not included in the present analysis, since the 2005/6 data set was too small to apply the multifrequency solutions in this paper. However, all the previously detected main frequencies were confirmed in the 2005/6 data set (except for a 1 cd^{-1} shift for the 10.869 cd^{-1} frequency, which can be understood as an alias of the small 2f harmonic of the dominant radial mode).

4. Photometric mode identification

4.1. Measured multicolor phase shifts and amplitude ratios

During its pulsation cycle, a star changes in temperature, radius, and geometrical cross section. The relative changes depend on the type of pulsation mode (e.g., gravity and pressure modes) as well as the spherical harmonic quantum numbers. It is possible to separate the effects by studying the light variability as a function of wavelength (multicolor photometry), radial velocity and changes in the spectroscopic line-profiles. For A and F stars, the phase shifts and amplitude ratios between two or more photometric bandpasses are a function of the pulsation ℓ value. Consequently, the available v and y data for EE Cam can be used for mode identifications by comparison with appropriate stellar models (see, e.g., Breger 2014 for a recent review). It is important to note that in A and F stars, the small phase shifts are the main discriminants; consequently, the method can only be applied to large data sets of high quality.

For the main frequencies, we have computed the amplitude ratios and phase shifts in the v and y passbands for each observing season. The results, listed in Table 2, are the weighted averages of the different observing seasons.

4.2. Theoretical modeling

We computed theoretical phase differences and amplitude ratios for a model based on the photometrically determined effective temperature and luminosity.

For the effective temperature we adopted the value from Ammons et al. (2006), i.e., 6469^{+65}_{-73} K, but assumed a higher uncertainty of 200 K, which is typical for such determinations. Our luminosity estimate is based on the parallax of van Leeuwen et al. (2007) of 4.34 ± 0.63 mas. Moreover, we took into account the photometrically determined surface metallicity of [Fe/H] = $0.24^{+0.12}_{-0.13}$ (Ammons et al. 2006) for the estimate of the bolometric correction in the V band. Consequently, the luminosity of EE Cam (in solar units) was determined to be $1.53^{+0.14}_{-0.12}$.

For the computation of the theoretical phase differences and amplitude ratios we assumed that EE Cam generally has a solar chemical composition and that the higher metallicity is only a surface effect. Consequently, the higher surface metallicity was only adopted for the atmosphere models, while for the general models the Asplund et al. (2009) solar-element mixture

Table 1. Frequencies and amplitudes in the Strömgren v and y filters.

	Frequency		Mode or ID	Amplitude in millimag							
	cd^{-1}	μHz		2006/7		2007/8		2008/9		2009/10	
				v	y	v	y	v	y	v	y
Dominant modes				±0.2	±0.2	±0.3	±0.2	±0.2	±0.2	±0.2	±0.1
f_1	4.9335	57.101		56.7	36.2	56.6	35.6	56.6	36.2	56.9	36.1
f_2	5.2138	60.345		31.2	19.8	31.4	20.0	31.9	20.3	32.0	20.6
f_3	8.3329	96.445		10.3	6.6	14.4	9.5	16.0	10.4	16.8	10.8
Additional modes: annual solutions											
f_4	4.3201	50.001		2.8	2.1	3.0	1.7	3.2	2.1	3.3	1.9
f_5	4.7645	55.144		3.9	2.7	4.5	2.8	4.2	2.9	3.7	2.3
f_6	4.9375	57.147		7.0	4.5	6.9	4.3	6.9	4.4	6.3	4.2
f_7	7.91[1]	91.5[1]		4.3	2.8	8.4	5.1	5.6[1]	3.4[1]	4.4	3.0
f_8	8.2653	95.664		3.3	2.1	4.0	2.6	3.8	2.6	3.8	2.6
f_9	8.4559	97.869		6.9	4.4	5.6	3.5	4.9	3.5	6.7	4.5
f_{10}	9.4761	109.677		3.3	2.1	5.5	3.9	6.7	4.3	4.3	2.7
f_{11}	9.8398	113.886		9.5	6.2	5.8	3.8	4.2	2.7	9.9	6.7
f_{12}	11.0339	127.707		1.9	1.1	2.5	1.6	5.4	3.7	5.1	3.4
Additional modes: overall solution				±0.1	±0.1						
f_{13}	3.4467	39.893		1.0	0.6						
f_{14}	4.7787	55.310		1.8	1.2						
f_{15}	5.3207	61.582		1.6	1.0						
f_{16}	6.0243	69.725		0.8	0.6						
f_{17}	6.2038	71.803		2.5	1.5						
f_{18}	6.8304	79.056		1.1	0.8						
f_{19}	7.0153	81.195		1.4	0.9						
f_{20}	7.3735	85.341		1.5	0.9						
f_{21}	7.6653	88.719		2.5	1.6						
f_{22}	8.0540	93.218		0.8	0.6						
f_{23}	8.1492	94.319		1.8	1.3						
f_{24}	8.5120	98.519		2.2	1.3						
f_{25}	9.5481	110.510		2.8	1.6						
f_{26}	9.8671	114.202	$2f_1$	3.5	2.4						
f_{27}	9.9590	115.266		2.3	1.5						
f_{28}	10.1143	117.063		1.2	0.8						
f_{29}	10.1474	117.447	f_1+f_2	4.2	2.8						
f_{30}	10.3179	119.420		1.7	1.2						
f_{31}	10.3427	119.707		1.3	0.8						
f_{32}	10.3986	120.354		1.3	0.8						
f_{33}	10.7708	124.662		1.8	1.0						
f_{34}	10.8459	125.531		1.5	1.0						
f_{35}	10.8748	125.866		1.7	1.0						
f_{36}	11.0201	127.547		1.1	0.8						
f_{37}	11.3210	131.031		1.4	0.9						
f_{38}	11.4743	132.804		1.1	0.7						
f_{39}	12.7113	147.122		1.2	0.7						
f_{40}	13.2664	153.546	f_1+f_3	1.0	0.7						

Notes. [(1)] The mode at 7.91 cd^{-1} showed a slightly variable frequency from year to year. We have adopted 7.9051 cd^{-1} (2006/7), 7.9065 cd^{-1} (2007/8), 7.9067 cd^{-1} (2008/9), and 7.9081 cd^{-1} (2009/10). During the 160d observing season in 2008/9, the amplitudes were systematically increasing from 3 to 9 mmag in v and 2 to 6 mmag in y.

(i.e., $X = 0.74$, $Z = 0.134$) was adopted. Moreover, our models are based on OPAL opacities.

The results of our computations are shown in Fig. 3. The diagram shows the theoretical values of phase differences and amplitude ratios of all $\ell \leq 2$ modes within the observed frequency range. Only observed modes with sufficiently small error bars are considered in the given diagram (i.e., f_1, f_2, f_3, and f_{10}). The dominant mode, f_1, is clearly identified as a radial mode, while f_2 can be interpreted as a dipole mode. The remaining two modes, f_3 and f_{10}, can be both dipole as well as quadrupole.

The theoretical and observed amplitude ratios tend to differ more for nonradial modes. The observed values are lower than the theoretical predictions and this is not only the case for the delineated modes but also for the modes with higher error bars (see Table 2). The relatively poor fit of amplitude ratios is not uncommon for δ Scuti and indicates minor flaws in our description of the stellar outer layers, e.g., the use of the rather simplistic mixing-length treatment of convection.

For the pulsation computations we adopt the frozen-in convection approximation, i.e., we neglect perturbations of the convective energy flux during the pulsation cycle. While these simplifications are reliable for relatively hot stars such as B stars, for the colder δ Scuti stars some interaction between convection and pulsation is expected. Regrettably, the exact value of the

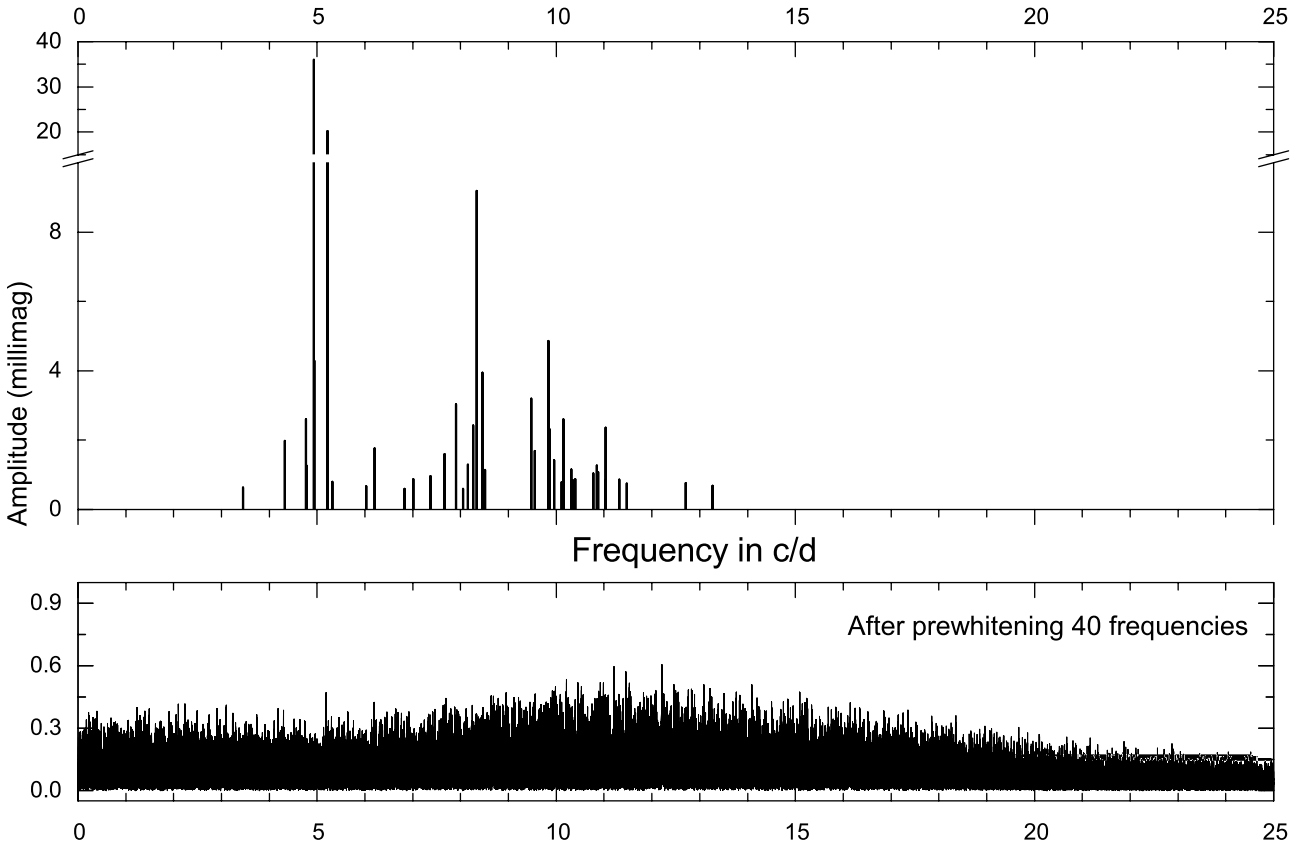

Fig. 1. *Top panel*: distribution of detected significant frequencies of EE Cam. *Bottom panel*: Amplitude spectrum of the residuals after 40 frequencies are subtracted. This shows that many additional small-amplitude pulsation frequencies are present, especially near the previously detected and prewhitened high frequencies. These peaks have an amplitude signal/noise ratio under the limit of 4.0. For these peaks we cannot separate instrumental noise from effects of nearby pulsation modes and spurious peaks caused by undetected amplitude variability.

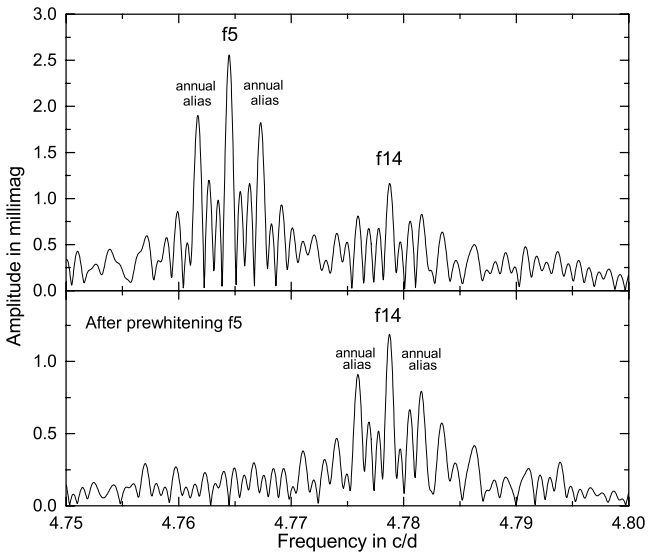

Fig. 2. Example of a detection of two close frequencies separated by about 0.013 cd^{-1}. The time base of 3.5 years leads to excellent frequency resolution, affected only by daily aliasing of 1.0 cd^{-1} and annual aliasing of 0.027 cd^{-1}.

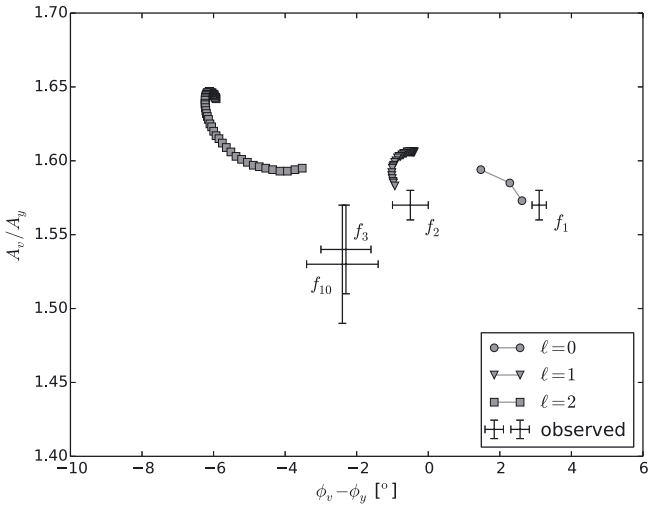

Fig. 3. Comparison between theoretical and observed phase differences and amplitude ratios.

temperature at which the transition from ineffective convection in hotter stars to effective convection in colder stars is located is still uncertain. In the case of a similar star, FG Vir, Daszynska-Daszkiewicz et al. (2005) found convection to be ineffective (see Fig. 7 in that paper). For EE Cam we also found the best agreement between theoretical and observed amplitude ratios and phase differences with a mixing length parameter smaller than 0.5.

Another uncertainty might arise from the rotation rate of EE Cam, which is roughly between those of the slowly and rapidly rotating δ Scuti stars. Most mode identification methods are valid only in the limit of slow to moderate rotation. For rapidly rotating stars, the geometric aspect changes because of

Table 2. Phase shifts and amplitude ratios in the v and y passbands.

	Frequency	Phase shift	Amplitude ratio
		$\phi_v - \phi_y$	v/y
	cd^{-1}	degrees	
f_1	4.9335	3.1 ±0.2	1.57 ±0.01
f_2	5.2138	–0.5 ±0.5	1.57 ±0.01
f_3	8.3329	–2.3 ±0.7	1.54 ±0.03
f_4	10.1474	1.1 ±1.1	1.46 ±0.15
f_6	4.3201	0.0 ±0.9	1.60 ±0.18
f_7	7.9051	–1.3 ±3.5	1.53 ±0.11
f_{10}	8.2653	–2.4 ±1.0	1.53 ±0.04
f_{11}	8.4559	–1.4 ±2.0	1.52 ±0.09
f_{12}	9.4761	–1.5 ±1.7	1.52 ±0.07

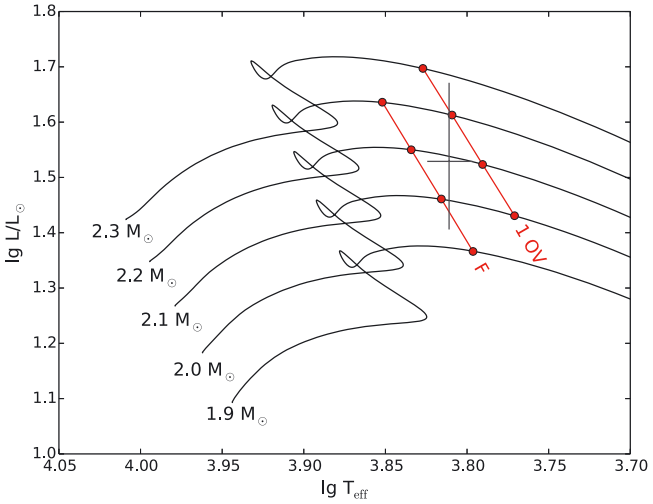

Fig. 4. Positions in the Hertzsprung-Russell diagram showing a comparison between the photometrically determined luminosity and effective temperature with those of models that fit f_1 as radial fundamental (F) and first radial overtone (1 OV), respectively.

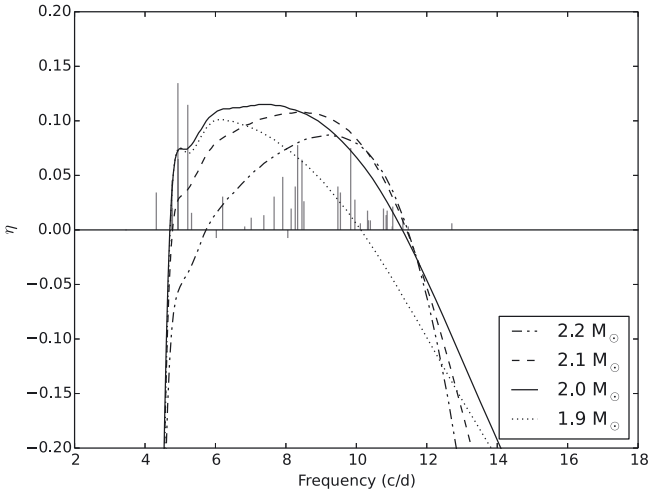

Fig. 5. Instability parameter, η, vs. frequency in comparison with the observed frequency spectrum. Positive η indicates unstable modes. The results are shown for models that fit f_1 as fundamental radial mode. An excellent agreement between observations and theoretical models is achieved for a 2.0–2.1 $M_\odot$ model.

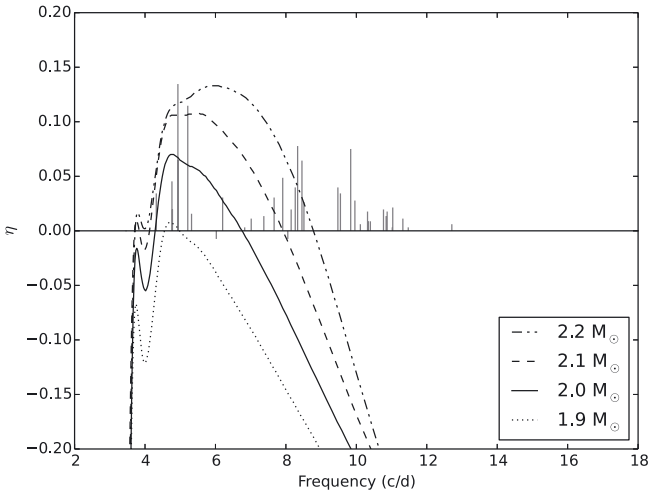

Fig. 6. Similar to Fig. 5, but presenting the case of models that fit f_1 as first radial overtone mode. None of these theoretical models match the observed range of mode instability.

the flattened shape, and the oscillation amplitudes are concentrated towards the equator (Lignières et al. 2006). In the case of EE Cam, however, the flattening should be still a minor effect. With an inclination angle of $i = 34 \pm 4$ degrees the visibility of axisymmetric modes is favored because of the geometric aspect (see Fig. 6 in Breger & Lenz 2008). These modes are less influenced by rotation than their non-axisymmetric counterparts. Consequently, the rotational velocity of EE Cam also should not introduce large uncertainties in our mode identifications.

The agreement of the present photometric mode identifications with those obtained from spectroscopic line-profile variations for three pulsation modes (Castanheira et al. 2014) is excellent. Both the radial pulsation of f_1 and $\ell = 1$ identification of f_2 are in perfect agreement. Furthermore, from photometry f_3 could be either $\ell = 1$ or 2, while the line-profile variations were matched with $\ell = 1$.

5. Discussion

Based on phase differences between the photometric v and y band the dominant mode, f_1, was identified as a radial mode. The radial order of f_1 cannot be determined by this technique, however. Using the Warsaw-New Jersey evolutionary code we constructed a grid of models and examined models which fit f_1 as a radial mode in more detail. The evolutionary tracks of these models in the Hertzsprung-Russell Diagram are shown in Fig. 4. In this diagram, pulsational models that fit f_1 as radial fundamental as well as radial first overtone are marked. The observed position of the star lies between the two models. Consequently, with this method f_1 could be identified with both the fundamental and the first overtone radial mode. To exclude one of these two possibilities, a more detailed study of these models is required.

There exists an additional method to distinguish between the radial fundamental and first overtone modes. Often a theoretical model can be excluded because the predicted frequency range of unstable modes does not match the observed unstable frequencies.

Consequently, we performed a detailed instability study on all models that fit f_1 as a radial mode. These models use a mass between 1.9 and 2.2 $M_\odot$. The results of this investigation are presented in Fig. 5 for models in which f_1 is the radial fundamental mode and in Fig. 6 for models in which f_1 is the first radial overtone mode. The instability ranges shown in these figures agree very closely with the identification of f_1 as the radial

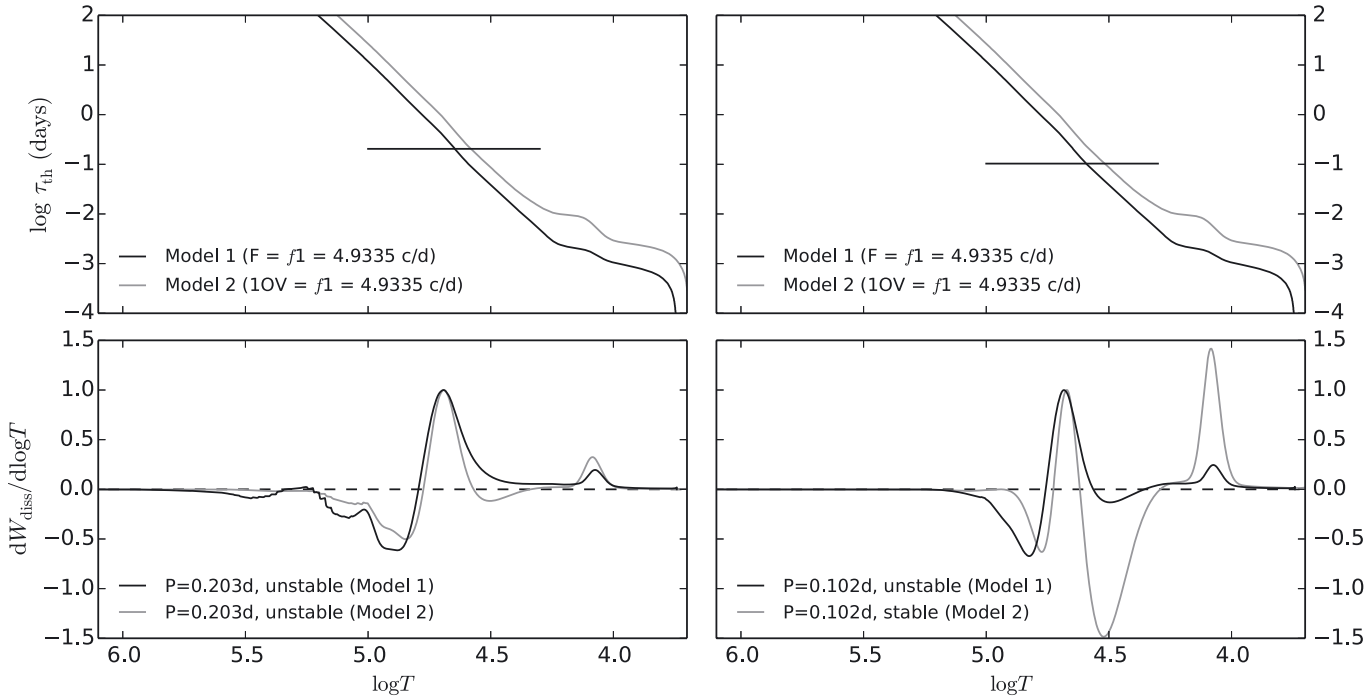

Fig. 7. *Upper panels*: behavior of the local thermal timescale in a model which fits f_1 as the radial fundamental (black line) and a model which fits f_1 as the first radial overtone (grey line). The horizontal lines mark the periods of selected modes (0.203 d in the *left panel* and 0.102 d in the *right panel*). *Lower panels*: differential work integral for the corresponding modes in the envelopes of both models (positive in driving zones, negative in damping zones).

Table 3. Theoretical model parameters.

f_1 fit	$\log M/M_\odot$	$\log L$	$\log T_{\rm eff}$
F	2.2	1.636	3.852
F	2.1	1.550	3.834
F	2.0	1.461	3.816
F	1.9	1.366	3.796
1H	2.3	1.697	3.827
1H	2.2	1.613	3.809
1H	2.1	1.523	3.790
1H	2.0	1.431	3.771

Notes. For all models OPAL opacities as well as the Asplund et al. (2009) solar element mixture of $X = 0.74$, $Z = 0.0134$ were adopted. Moreover, for the mixing-length parameter, $\alpha_{\rm MLT}$, 0.2 as well as 0.5 were used. The overshooting parameter, $\alpha_{\rm ov}$, was fixed at 0.1. Uniform rotation was assumed with values within the range 72 ± 10 km s^{-1}.

fundamental mode and disagree with an identification as the first radial overtone.

This conclusion results from the significant difference in the theoretical instability of higher-frequency modes (e.g., modes with frequencies above 10 cd^{-1}). These frequencies are unstable in models that identify f_1 with the radial fundamental mode (Fig. 5), but stable in the first overtone-mode models (Fig. 6).

The reason for this effect becomes clear if we compare the local thermal timescales in these two families of models with the corresponding periods of the modes. The comparison of these quantities, as well as the differential work integral, is presented in Fig. 7 for the fundamental mode and first overtone mode models of 2 $M_\odot$. The left panels show the instability of lower frequency modes of 4.9 cd^{-1}. With a period of 0.203 d, these are radial modes p_1 and p_2 in the fundamental mode and first overtone mode models, respectively. The right panels delineate the same for modes closer to the higher frequency end of the observed frequency spectrum. With frequencies of 9.8 cd^{-1} (period 0.102 d), the corresponding high-frequency modes would be the radial modes p_4 and p_6 in the two types of models, respectively.

To excite an oscillation mode, the thermal timescale in the driving zone has to be comparable or longer than the oscillation period (Pamyatnykh 1999). The layers in the stellar envelope, where the local thermal timescale is comparable with the period of a mode under consideration, are the most important layers for the driving and damping of this mode. Deeper layers are less important owing to their adiabaticity, and higher layers are close to thermal equilibrium during the pulsation cycle. We can see that because of differences in the structure, for a fixed temperature value in the envelope, the local thermal timescale of the first overtone mode model is systematically higher than that of the fundamental mode model. Therefore, for a given oscillation period, the higher stellar layers will be important for the driving and damping of the oscillations. We can see that for the frequencies which correspond to the higher end of the observed frequency spectrum (right panels), the damping above the HeII ionization zone (which is located at a temperature of about 50 000 K in both models) will be more significant in the first overtone mode models than in the fundamental mode models. Therefore, these frequencies will not be driven in the first overtone mode models. For lower frequencies (left panels) this effect is small. Therefore, at low frequencies the selected mode is unstable in both models. Although uncertainties in convective efficiency may slightly modify the high-frequency end of the instability range, our result points to the identification of f_1 as the radial fundamental mode.

In this paper we adopt the previously published temperature of 6461 K. For the spectroscopic mode identification,

Castanheira et al. determined a temperature of 7110 K. This temperature difference has only a small effect on the spectroscopic mode identification, because the observed line-profile variations are mainly governed by the varying surface velocity field. In a similar analysis of the δ Sct star 4 CVn, Schmid et al. (2014) showed that the spectroscopic mode identification technique is not suited to constraining the global and atmospheric parameters of the star. In addition, if we consider the effects of temperature on our models for mode identification discussed above, the higher effective temperature from spectroscopy would further strengthen our result that f_1 is the radial fundamental mode.

The majority of δ Scuti stars are fast rotators with rotational velocities of $v \geq 100$ km s^{-1}. This group has small amplitudes of pulsation in the millimag range and, where identified, the dominant modes are nonradial. On the other hand, for the variables with $v \leq 30$ km s^{-1}, the radial pulsation modes are usually dominant with large amplitudes: these stars with peak-to-peak amplitudes of 300 mmag or larger are also known as the HADS. However, even in this group, a small number of pulsators show small amplitudes (see Fig. 5 in Breger 2000). EE Cam belongs to the rotationally intermediate group. This star shows that the amplitudes are indeed smaller than those of the HADS, but also that the highest-amplitude mode can still be radial, followed closely by a nonradial $\ell = 1$ mode. This behavior is compatible with the hypothesis that increasing rotational velocities are associated with decreasing amplitudes of the radial modes. On the other hand, in EE Cam, the large number of excited nonradial modes mirrors that of the fast-rotating group.

Acknowledgements. M.B. is grateful to the Austrian Fonds zur Förderung der wissenschaftlichen Forschung for supporting both the research and the publication costs of this investigation. A.A.P. acknowledges partial financial support from the Polish NCN grant 2011/01/B/ST9/05448. V.S.S. is supported as an Aspirant PhD fellow of the Fonds voor Wetenschappelijk Onderzoek, Vlaanderen (FWO), Belgium.

References

Ammons, S., Robinson, S., Strader, J., et al. 2006, ApJ, 638, 1004
Asplund, M., Grevesse, N., Sauval, A. J., & Scott, P. 2009, ARA&A, 47, 481
Breger, M. 2000, ASP Conf. Ser., 210, 3
Breger, M. 2014, Proc. IAU Symp., 301, 93
Breger, M., & Hiesberger, F. 1999, A&AS, 135, 547
Breger, M., & Lenz, P. 2008, A&A, 488, 643
Breger, M., Stich, J., Garrido, R., et al. 1993, A&A, 271, 482
Breger, M., Rucinski, S.M., & Reegen, P. 2007, AJ, 134, 1994 (Paper I)
Breger, M., Balona, L., Lenz, P., et al. 2011, MNRAS, 414, 1721
Castanheira, B. G., Elmasli, A., Schmid, V., et al. 2014, AJ, submitted
Daszyńska-Daszkiewicz, J., Dziembowski, W. A., Pamyatnykh, A. A., et al. 2005, A&A, 438, 653
Koch, D. G., Borucki, W. J., Basri, G., et al. 2010, ApJ, 713, L79
Koen, C. 2001, MNRAS, 321, 44
Lenz, P., & Breger, M. 2005, CoAst, 146, 53
Lignières, F., Rieutord, M., & Reese, D. 2006, A&A, 455, 607
Pamyatnykh, A. A. 1999, Acta Astron., 49, 119
Perryman, M. A. C., et al. 1997, The HIPPARCOS and Tycho Catalogues (Noordwijk: ESA) ESA SP, 1200
Schmid, V. S., Themessl, N., Breger, M., et al. 2014, A&A, 570, A33
Strassmeier, K. G., Boyd, L. J., Epand, D. H., & Granzer, T. H. 1997, PASP, 109, 697
van Leeuwen, F. 2007, A&A, 474, 653